Available online at **www.joac.info**

ISSN: 2278-1862

Journal of Applicable Chemistry

2019, 8 (3): 1001-1011

(International Peer Reviewed Journal)

Photocatalytic Applications of Semiconducting Metal oxide Materials-A Review

D. Nathiya[1], N. M. I. Alhaji[1]*, M. Kavin Micheal[2], Mayuri Meshram[2,3] and A. Ayeshamariam[2]

1. Department of Chemistry, Khadir Mohideen College, Adirampattinam-614701, **INDIA**
2. Department of Physics, Khadir Mohideen College, Adirampattinam-614701, **INDIA**
3. Integrated Science Education and Research Centre (ISERC), Santiniketan, Bolpur, West Bengal-731235, **INDIA**

Email: nmialhaji34@gmail.com

Accepted on 25th April, 2019

ABSTRACT

Semiconducting metal oxides are one of the important materials of a special attention with photocatalytic properties to clean water and preserve plants. To remove the impurities and dyes from effluents water technological approaches take the important tool to perform the purification on photocatalytic surfaces. Metal oxides such as ZnO, WO_3, TiO_2, CeO_2 AgO, Ga_2O_3, $AgGaO_2$ and $ZnGa_2O_4$ use their photocatalytic properties to clean water and soil and to inhibit the growth of undesirable micro-organisms, mold, algae, lichens and fungi. This review focuses about the reported research analyses of based on photocatalytic properties of metal oxides.

Graphical Abstract

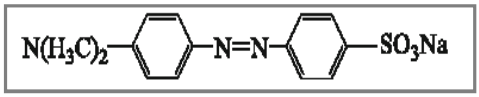

Methyl orange

Keywords: Photocatalytic degradation, Water purification, Semiconducting oxides, Metal oxides.

INTRODUCTION

The photocatalytic applications for environmental purification employ visible light sensitive photocatalysts, which efficiently use visible light from Sun source. The highly dispersed valence band leads to a small effective mass of the holes with a higher hole mobility. The effective hole conduction and relatively large band gaps are advantageous to the p-type conductivity, transparency, and photocatalytic activity. The indirect band gap of R-$AgGaO_2$ agrees well with reported results of electronic structures with a conduction band minimum on the point and a valence band maximum. The free charge carriers are photogenerated in a semiconductor and rapid communications between the different sub band states in the valence band and conduction band are complete, then the photo carriers will occupy the lowest states in their corresponding bands (i.e., they become thermalized). The carrier temperature becomes equal to the ambient temperature and the carriers are

indistinguishable, regardless of the initial state immediately occupied upon photo excitation, on the structural properties and photocatalytic activities [1].

Ag_2O has O-Ag-O dumbbell bonds and the electronic structure of Ag_2O has a highly dispersed valence band, its band gap is almost zero (not shown), which may be due to the O-Ag-O three-dimensional cross-linking as Cu_2O. In contrast, silver complex-oxides, including Ag^+ ions such as $AgNbO_3$, have relatively large band gaps. However, the bonds and the interactions between the Ag+ ion and O^{2-} ions are weak, which decrease the dispersion of the calculated valence band and lower the hole conductivity. Thus, the weak bonds and interactions may explain the low photo oxidation activity of these silver complex-oxides. However, R-$AgGaO_2$ is an excellent photocatalyst, which is sensitive to visible light, because it has the appropriate band gap for visible light absorption and a high hole conductivity, which both originate from its unique layered crystal structure [2].

ZnO based photocatalysts: ZnO is a representative n-type semiconductor with a wide band gap of 3.37 *eV* and a high excitation binding energy of 60 *meV* which produces electron–hole pairs under UV light or visible light irradiation. ZnO is the most common material that is being used as photocatalysis for the degradation of organic pollutants. Chen *et al.*, [3] synthesized ZnO nanoparticles (NPs) by sol–gel method using zinc acetate as precursor material. ZnO NPs was obtained via thermal treatment at different calcination temperatures of 300, 400, 500, and 600°C. Different composite ratios (molar ratio of oxalic acid to zinc acetate), ranging from 2 to 5, were prepared while keeping the ratio of zinc acetate at 0.01 mole. The photocatalytic activity of ZnO was determined using the degradation of azo dyes such as MO, CR, and DB38. Results showed that the removal rate of azo dyes increased with the increased dosage of catalyst and decreased initial concentration of azo dyes and the acidic condition is favorable for degradation. Thus, the economical and environment-friendly photocatalyst can be applied to the treatment of wastewater contaminated with synthetic dyes.

Nekouei *et al.*, [4] proposed the synthesis, characterization, and photocatalytic accomplishment of ZnO nanoplate (ZnOs) modified with activated carbon derived from Konar bark. The synergic efficiency of ZnO-AC exhibited a good rate of ciprofloxacin (CIP) removal under visible irradiation. In addition, first pseudo order kinetic and isotherms equations were calculated. Moreover, the identification of degradation products was performed by ultra performance liquid chromatography-tandem mass spectrometer (UPLC-MS/MS). It is for the first time that a ZnO photocatalyst modified with activated carbon (ZnO-AC) applied for CIP degradation.

Atchudan *et al.*, [5] synthesized the hybrid composite of ZnO nanoparticles decorated nitrogen-doped graphitic carbon sheets (ZnO@N-C) alongside nitrogen-doped carbon dots (N-CDs) were synthesized by the direct hydrothermal method of peach fruit juice and ZnO nanoparticles (ZnO NPs). Methylene blue (MB) degradation was estimated utilizing the ZnO@N-C hybrid composite, a maximum degradation efficiency of >95% was achieved in a neutral aqueous medium within 60 min under UV-light irradiation. This maximum efficiency allows estimating the contribution of the heterogeneous and homogeneity of ZnO@N-C hybrid composite which is responsible for the MB-degradation. Moreover, the economic natural biosource or bio-waste was employed for the synthesis of ZnO@N-C hybrid composite and displays an excellent photocatalytic degradation under UV-light irradiation which is an alternate for other carbon-based metal oxides. In addition, the resulting N-CDs were utilized as a fluorescence probe for cellular imaging, owing to their tremendous properties such as bright fluorescence with high quantum yield, excellent water solubility, and good biocompatibility.

Hassan *et al.*, [6] prepared zinc oxide nanoparticles using the extract of *Coriandrum sativum* leaf, and utilized as an effective photocatalyst for anthracene degradation at ambient temperature (25°C), pH 7 and ultraviolet irradiation for 240 min. Under these conditions the percentage decomposition of anthracene is ~96%. The kinetic study of the reaction obeys Langmuir–Hinshelwood model and fitted the pseudo first order rate constants. Formation of anthraquinone as a main decomposition product was confirmed by HPLC and gas–mass-spectrometry. This photocatalytic degradation reaction

significantly reduces the toxicity of anthracene. It is concluded that the photocatalytic degradation of anthracene with ZnO NP's prepared using the extract of *Coriandrum sativum* plant is an effective method in terms of simplicity, degradation efficiency and time of degradation.

Bae *et al.,* [7] reported the synthesis of zinc oxide-copper (I) oxide hybrid nanoparticles as colloidal forms bearing copper (I) oxide nanotubes bound to zinc oxide spherical cores. These nanoparticles utilized as photocatalysts for the direct conversion of carbon dioxide to methane in an aqueous medium, under ambient pressure and temperature. The catalysts produce methane with an activity of 1080 μmol g cat $^{-1}$ h^{-1}, a quantum yield of 1.5% and a selectivity for methane of >99%. The catalytic ability of the zinc oxide-copper(I) oxide hybrid catalyst is attributed to excellent band alignment of the zinc-oxide and copper(I) oxide domains, few surface defects which reduce defect-induced charge recombination and enhance electron transfer to the reagents, and a high-surface area colloidal morphology.

Turkyılmaz *et al.,*. [8] synthesized ZnO and different transition metal doped ZnO nanostructures by hydrothermal method. The optical band gap value was calculated as 3.24, 3.15, 3.10, 3.05 and 3.00 *eV* from UV–Vis diffuse reflectance spectra of ZnO, Ag/ZnO, Ni/ZnO, Fe/ZnO and Mn/ZnO photocatalysts, respectively. The results of the photocatalytic degradation of tartrazine in aqueous solutions under the UV-light showed that Ni/ZnO exhibited higher photocatalytic activity than the other ones. Mn/ZnO demonstrated the lowest photocatalytic activity among the synthesized photocatalysts. Thus, Ni and Ag exhibited synergistic effect while Fe and Mn exhibited antagonistic effect on the ZnO photocatalytic activity. The maximum degradation rate of tartrazine was obtained to be 98.2% in the 60 min using Ni/ZnO.

The enhanced photocatalytic performance of Ag_2S@ZnO hybrid photocatalyst was achieved under sonication by taking advantage of the piezotronic effect [9]. Decorating Ag_2S (~1.4 *eV* band gap) nanoparticles on ZnO (~3.3 *eV* band gap) nanowire surfaces successfully extended the light response to the visible light range. Furthermore, the strain-generated positive piezocharges effectively lowered the barrier height, considerably motivating charge transport across the Ag_2S/ZnO heterointerface, which further boosted the hybrid photocatalyst performance. The high reproducibility of the photocatalytic activities indicated that the modification of ZnO nanowires with Ag_2S nanoparticles effectively stabilized the photocatalyst in reactions. The degradation rate of Ag_2S@ZnO nanowires remained at C/C_0 = 18.6% after eight cycles, while bare ZnO nanowires exhibited poorer performance (C/C_0 = 48.1%). This study showed the effectiveness of using the piezotronic effect in water purification and recovery by combined use of solar and mechanical energy.

Porous ZnS, ZnO and ZnS–ZnO NSs are successfully synthesized via simple thermal annealing of ZnS(en)0.5 complex precursor in air atmosphere [10]. ZnS–ZnO NSs exhibit the highest photocatalytic activity and good photocatalytic stability in the decomposition of organic dye molecule rhodamine B (RhB) under ultraviolet (UV) light illumination due to their biggest specific surface area and special hetero structure.

The improved solar light photocatalytic movement of the ZnO/ZCIS composite has been achieved with the increased lifetime of charge carrier transfer and by the increased light absorption in the visible region due to the hetero junction created between the ZCIS QDs and ZnO nanoparticle. Rock salt phase with large fractions of oxygen vacancies is successfully stabilized at ambient conditions by inducing plastic strain in pure ZnO under 6 GPa using the High-Pressure Torsion (HPT) method [11].

Formation of rock salt phase reduces the band gap of ZnO to 1.8 *eV*, which is in good agreement with the first-principles calculations, and significantly improves the photocatalytic activity under visible light. This is due to wide band gap of pure ZnO with wurtzite crystal structure (3.1–3.4 *eV*) limits its photocatalytic activity to the ultraviolet (UV) region of solar spectrum. High-pressure rock salt polymorph of ZnO shows narrow band gap; however, the rock salt phase is unstable at ambient pressure.

Hong *et al.*. [**12**] Observed high piezo-photocatalytic efficiency of degrading organic pollutants using CuS/ZnO nanowires by both solar and mechanical energy. CuS/ZnO heterostructured nanowire arrays are compactly aligned on stainless steel mesh by a two-step wet-chemical method. The nanocomposite facilitates an efficient light harvesting due to large surface area and easily removed from the treated solution. The ultrasonic assistance can greatly enhanced the photocatalytic activity due to the coupling of built-in electric field of hetero structures and piezoelectric field of ZnO nanowires. The utility of carbonaceous materials for hybrid semiconductor photocatalyst has been increasing rapidly due to the synergetic effect via interfacial charge transfer reactions.

Thangavel *et al.*, [**13**] synthesized novel graphdiyne-ZnO nanohybrids by the hydrothermal method and evaluated its photocatalytic activity on the degradation of azo dyes. The rate constant of these nanohybrids is 2-fold higher compared to that of the pure ZnO. Four different nanocomposites of AuAgZnO with differing compositions of silver and gold were made by solution combustion method [**14**]. These nanocomposites were formed as nanospheres. The composites contained bimetallic AuAg particles on the surface of ZnO semiconductor, the interface being silver. The amount of gold dominates the AuAg indicating the presence of only a thin layer of silver below gold causing a blue-shifted gold plasmon band and red-shifted silver plasmon band in comparison to their pure entity. The number of oxygen vacancies in ZnO as seen in EPR depends on AuAg metal content effects the photocatalytic deprivation of the Rhodamine-B & the photocatalytic production of hydrogen. The inter particle interaction of Ag with Au and ZnO also plays a major role in photocatalytic process. Results confirmed that Ag/ZnO/γ-Al_2O_3 nanofibers are a promising adsorbent for the removal of methyl orange and Cr(VI) ions and the adsorbent can be sustainably reused. Rare earth metal doping into semiconductor oxides is considered to be a useful approach to improve photocatalytic activity due to its ability in the direction to hold back the electron–hole pair recombination upon excitation [**15**].

Alam *et al.*, [**16**] reported the production of different rare earth metal (La, Nd, Sm and Dy)-doped ZnO nanoparticles using a facile sol–gel route followed by evaluation of their photocatalytic activity by studying the degradation of methylene blue (MB) and Rhodamine B (RhB) in UV-light irradiation. All metal doped ZnO showed improved photocatalytic activity toward the degradation of MB, of which, Nd-doped ZnO showed the best activity with 98% degradation efficiency. In addition, mineralization of the dye was also observed, indicating 68% TOC removal in 180 min with Nd-doped ZnO nanoparticles. Hollow ZnO microspheres were successfully synthesized by a one-step template-free hydrothermal synthetic route straightforwardly just for 30 min at 90°C. Hexamethylenetetramine and trisodium citrate played a significant role in the fabrication of hollow ZnO microspheres, and distilled water served as the main solvent without adding any organic solvent and surfactants. With the morphological evolution apperceived in the time-dependent growth of hollow ZnO microspheres, a possible formation mechanism based on Ostward ripening inside-out was proposed. Then, polyacrylate/hollow ZnO composite latex was obtained by physical blending of hollow ZnO microspheres and polyacrylate emulsion. As expected, hollow ZnO microspheres has a significant impact on water vapor permeability, water resistance and mechanical properties. Among them, the water vapor permeability and water resistance was relatively increased by 71.18% and 38.42%, respectively.

Zhang *et al.*, also prepared flower-like WO_3 photocatalyst with ultrathin nanosheets and the thickness of sheets is only 10 nm. In addition, the Ag nanoparticles deposition happening the exterior of WO_3 flowers in order to increase the visible-light absorption of WO_3 by effect of surface plasmon resonance (SPR). They further studied the photocatalytic activity of Ag@WO_3 photocatalyst towards the degradation of MB and 2-chlorophenol under the visible-light irradiation. The obtained degradation results exhibited that Ag@WO_3 photocatalyst was found to be degraded more dye molecules than the pure WO_3 photocatalyst [**17**].

Wang *at al.*, developed the Ag_3PO_4/WO_3 hybrid photocatalyst for investigating its visible-light photocatalytic ability towards the degradation of methylene blue (MB). Also, they observed that the

Ag_3PO_4/WO_3 hybrid achieved a progressive photocatalytic activity than pure Ag_3PO_4 and WO_3 [**18**]. Recently, Cao *et al.,* [**19**] prepared the novel $AgIO_3/WO_3$ composites from hydrothermal and chemical precipitation method with different amount of $AgIO_3$. The photocatalytic performance of these $AgIO_3/WO_3$ composites was investigated towards the deprivation of RhB under the visible-light irradiation. It revealed that 50% $AgIO_3/WO_3$ composites possesses a highest photocatalytic performance than the pure $AgIO_3$ and WO_3. This may be due to the fast separation and migration of photogenerated electron-hole pairs at the interface of $AgIO_3$ and WO_3.

Wang *et al.,* prepared metastable hexagonal WO_3 (h-WO_3) from a hydrothermal reduction method with glycerol and then, the Ag_3PO_4/h-WO_3complexes were prepared by a modest precipitation method. They found that the Ag_3PO_4/h-WO_3 photocatalyst showed an outstanding photocatalytic activity for degradation of methyl orange (MO) under the visible-light illumination than the Ag_3PO_4/h-WO_3. Also, the Ag_3PO_4/h-WO_3 composites exhibited a good stability compared with the pure Ag_3PO_4 which makes clear that the obtained h-WO_3 played a vital role in the degradation process [**20**].

Wang *et al.,* synthesized a novel visible-light-driven AgI/WO_3 nanocomposites using facile precipitation method. The photocatalytic activities of the AgI/WO_3 nanocomposites were premeditated by the deprivation of tetracycline hydrochloride (TC) under the visible-light illumination. They found that an optimized 20%-AgI/WO_3 revealed a highest photocatalytic performance than that of pure AgI and WO_3. Also, the stability test indicates that the better photostability of AgI/WO_3 nanocomposite [**21**].

Xu *et al.,* prepared three-dimensionally ordered macroporous WO_3 (3DOM WO_3) modified Ag_3PO_4 photocatalysts with the different 3DOM WO_3 contents. Furthermore, they studied their photocatalytic performance meant for degradation of methylene blue (MB) under the illumination of visible-light. The obtained degradation results were found to be showed that 4 wt% 3DOM WO_3-Ag_3PO_4 photocatalyst displayed a maximum photocatalytic performance than the pure 3DOM WO_3 and Ag_3PO_4. This enhancement may be due to the synergistic effect between the 3DOM WO_3 and Ag_3PO_4 and also increased the separation efficiency of the photogenerated electron-hole pairs after introduction of 3DOM WO_3 [**22**].

In addition, Lu *et al.,* also synthesized direct Z-scheme type WO_3/Ag_3PO_4 composite photocatalyst via hydrothermal method. Then, they evaluated their photocatalytic ability towards the degradation of the methylene blue (MB) and methyl orange (MO) under the illumination of visible-light and observed an enhanced photocatalytic activity for WO_3/Ag_3PO_4 composite photocatalyst when compared with pure Ag_3PO_4 and pure WO_3. The rate constant values of MB and MO degradation over WO_3/Ag_3PO_4 composite were about 2.4 and 2.5 times higher than that of the pure Ag_3PO_4, respectively. This improved photocatalytic activity of WO_3/Ag_3PO_4 composite also owed to the synergistic effect together with relatively large surface area, strong absorption oflight ability, matched energy band level and an efficient parting of photogenerated charge carriers between the Ag_3PO_4 and pure WO_3 [**23**].

Chen *et al.,* synthesized the hierarchical of Ag/AgCl@WO_3 nanoplate with an advanced photocatalytic activity towards the visible-light degradation of RhB from aqueous solutions than the Ag/AgCl, AgCl, AgCl@WO_3 and TiO_2 (P25) **[24**].

Yao *et al.,* synthesized cuboid rods of monoclinic WO_3 (m-WO_3) using preoxo-polytungstic acid as the precursor through a hydrothermal method. Furthermore, they synthesized AgBr/m-WO_3 composite photocatalysts with varying loadings of AgBr for the photocatalytic degradation of RhB, MO and MB under visible-light irradiation. Among the different composites, the AgBr/m-WO_3 with 30 wt% of AgBr showed the highest photocatalytic activity than the others [**25**].

Yuan *et al.,* developed a novel Z-scheme $Ag_2CO_3/Ag/WO_3$ composite via a facile deposition and photochemical reduction method. They investigated their photocatalytic activity towards the

degradation of RhB, MO, ciprofloxacin (CIP) and tetracycline hydrochloride (TC) under visible-light irradiation. It showed that $Ag_2CO_3/Ag/WO_3$ composites have the developed photocatalytic activity compared with that of the pure Ag_2CO_3 rods and WO_3 nanoparticles. The efficient photocatalytic activity of these complexes may be due to large portion of the visible light absorption by a surface plasmon resonance (SPR) effect, effective separation of photogenerated charge carriers and also the formation of a Z-scheme system [**26**].

Yan *et al.,* achieved a novel Ag_3VO_4/WO_3 composite by the hydrothermal and a facile precipitation method. This composite material was further used by the way of photocatalyst for the degradation of tetracycline (TC) under the visible-light illumination. The results revealed that Ag_3VO_4/WO_3 composite exhibited excellent photocatalytic ability than the pure Ag_3VO_4 and WO_3 [**27**].

Adhikari *et al.,* synthesized the $Ag/AgCl/WO_3$ composite photocatalyst via a microwave assisted hydrothermal method. This composite photocatalyst showed a higher photocatalytic performance towards the deprivation of RhB under replicated solar light irradiation. Also, the degradation efficiency of this composite photocatalyst was enhanced largely when compared with commercial WO_3 nanopowder which mainly accredited to the surface plasmon resonance (SPR) effect caused by the Ag nanoparticles present in the composite photocatalyst [**28**].

Zhu *et al.,* [**29**] reported $Ag/\beta\text{-}Bi_2O_3$ microspheres via simple chemical technique. The photocatalytic activity of the compound was assessed towards degradation of RhB dye under the visible light radiation. It is concluded that the photocatalytic degradation was enhanced for Ag loaded $\beta\text{-}Bi_2O_3$ than that of pure $\beta\text{-}Bi_2O_3$ which is due to the structure of the material which favored migration of electron-hole pairs, leading higher photocatalytic activity. Similarly, Ag doped Bi_2O_3 photocatalyst [**30**] with different molar ratio of Ag/Bi (3, 5, 7 and 9%) have been prepared through co-precipitation and evaluated for the photo-degradation of MO.

It was noticed that 3 mol% Ag doped Bi_2O_3 exhibited higher photocatalytic activity over the pristine and all the other samples under visible light irradiation. $Au/\alpha\text{-}Bi_2O_3$ microrods with different Au loadings have been fabricated by depositing-precipitation method. The visible light photocatalytic activities of $\alpha\text{-}Bi_2O_3$ microrods for the degradation of RhB and 2, 4-DCP in aqueous solutions can be significantly enhanced by loading Au on the surface. The highest photocatalytic activity was reached on 1.0 wt% $Au/\alpha\text{-}Bi_2O_3$. The Au loaded on $\alpha\text{-}Bi_2O_3$halls a significant role in the separation of the photo-generated electron–hole pairs by accumulating the electrons from the excited $\alpha\text{-}Bi_2O_3$ substrate [**31**]. Azo dyes formula and structures are shown in figure 1(a-c)

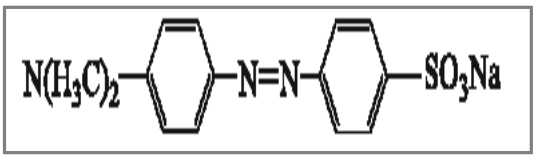

(a). Methyl orange, $C_{14}H_{14}N_3SO_3Na$

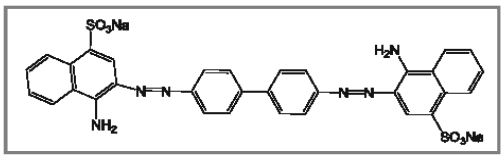

(b). CR. $C_{32}H_{22}N_6NaO_6S_2$

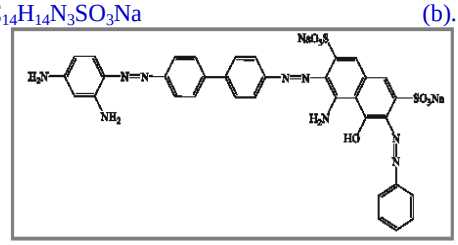

(c). DB 38. $C_{34}H_{25}N_9Na_2O_7S_2$

Figure 1 (a-c). Molecular Formula and Structure of Azo dyes.

CeO_2 based Photocatalysts:

Material(s)	Shape	Preparation method	Dyes used	Diameter/crystal size, nm	Length, µm	Reference
CeO_2	Nanorod	Solvothermal synthesis	--	40-50	0.3-2	[32]
CeO_2+ Na_3PO_4	Nanorod	Hydrothermal process	1,2,4-trichloro-benzene	5-10	1-2	[33]
Polyhedral shapes of CeO_2	Nanoparticle	Hydrothermal process	--	3-10	--	[34]
$CeOHCO_3$ and CeO_2	Nanorod	Sonochemical method	--	100-150	300-400	[35]
CeO_2 catalyst for $deNO_x$	Nanoscale	Hydrothermal / precipitation method	--	10-20	--	[36]
$Ce(NO_3)_3.6H_2O$	Nanospheres	Hydrothermal process	--	100-250	--	[37]
Polycrystalline CeO_2	Nanowire	Solution-phase route	--	30-120	0.2-5	[38]
Colloidal CeO_2	Nanocrystal	Hydrothermal synthesis	--	--	67	[39]
Undoped Ceria	Nano-powders	Hydrothermal method	--	12-16	--	[40]
Doped Ceria with Rare Earth (RE=Pr, Gd and Sm)	Nanoparticles	Hydrothermal method	--	13-25	--	[41]
CeO_2	Hollow sphere	Photocatalytic activity	--	60	--	[42]
CeO_2 composed of numerous fluorite cubic single crystal	Nanorod	Hydrothermal process	--	20-40	upto several µm (1-2 µm)	[43]
Ultrafine CeO_2	Nanoparticles	--	CI Reactive Black 5	< 6	--	[44]
$SrTiCO_3/CeO_2$		Photocatalysis	--	50-100	--	[45]
CeO_2 NPs	Nanoparticles	Hydrothermal / precipitation method	CI Reactive Black 5	8-10	--	[46]
CeO_2	Nanobelts	Cost-effective hydrothermal method	MO	20	--	[47]
Sm^{3+}/Eu^{3+} co-doped with CeO_2	Nanocrystals	Oxalate decomposition method	--	4-6	--	[48]
Cds NPs+ CeO_2 NRs	Nanoparticles	Catalyst preparation (Hydrothermal method)	--	5-10	0.1 – 0.5	[49]
BTO+ CeO_2	Nanoparticles	Photocatalysts	--	10-60	--	[50]
Ce-ZrO_2	Nano-fibrous web	Electrospinning method	--	10-50	--	[51]
CeO_2	Nanowires	Facile synthesis	CR	10-50	upto several µm	[52]
CeO_2	Nanosheets	Precipitation process	--	--	Tens of µm	[53]
CeO_2	Nanoparticles	One-step ultrasound synthesis	--	--	--	[54]
$BiVO_4$/ CeO_2	Nanocomposite	Homogenous precipitation with hydrothermal technique	MB, MO and mixture of these two	--	--	[55]

APPLICATION

ZnO, WO_3, TiO_2, CeO_2 AgO, Ga_2O_3, $AgGaO_2$ and $ZnGa_2O_4$ these compounds are used in the preparation of arc carbons to increase brilliance. These are commonly used as heat resistant alloy coatings and in ceramic coating. For the production of hydrogen and waste water treatment these are the promising candidates. These compounds very much helpful in Antioxidant activity, Anticancer activity, Cytotoxicity, Antibacterial activity, Neurotoxicity and Genotoxicity. These are the sources for additives in glass, fuel poilishing agents and UV protecting products, scintillation counters, drugs and pharmaceuticals

CONCLUSION

Extensive investigations have been explored by several research groups on the fundamental aspects of development, modification and utilization of metal oxide based heterostructured materials as photocatalysts for deprivation of the organic pollutants. In this review, we have concised the topical developments in metal oxide based heterostructures for photocatalytic applications towards environmental remediation. The special attention has been made on different metal oxide materials under various categories such as ZnO, WO_3, TiO_2, CeO_2 AgO, Ga_2O_3, $AgGaO_2$ and $ZnGa_2O_4$ based photocatalysts. The metal oxide based heterostructures are promising materials for environmental remediation because of their unique physical and chemical properties, stable, inexpensive and tunable band energy with high visible light absorption nature, which originates to the enhanced catalytic performance. This review focuses on major challenges of degradation and water purification based on numerous reports which dealt with an advancement of metal oxides-based visible-light driven photocatalysis for the environmental remediation applications.

REFERENCES

1. H. Irie, Y. Watanabe, K. Hashimoto, Nitrogen-concentration dependence on photocatalytic activity of $TiO_{2-x}Nx$ powder, *The Journal of Physical Chemistry B*, **2003**, 107(23), 5483-5486.
2. X. Chen, Z. Wu, D. Liu, Z. Gao, Preparation of ZnO photocatalyst for the efficient and rapid photocatalytic degradation of azo dyes, *Nanoscale research letters*, **2017**, 12(1), 143-153.
3. S. Nekouei, F. Nekouei, H. Kargarzadeh, Synthesis of ZnO photocatalyst modified with activated carbon for a perfect degradation of ciprofloxacin and its secondary pollutants, *Applied Organometallic Chemistry*, **2018**, 32(3), 4198-4208.
4. G. A. Korteweg, Determination of spin-Hamiltonian parameters from EPR powder spectra of Fe (HI) substituted in β-$AgAlO_2$ and β-$AgGaO_2$, *Journal of Magnetic Resonance*, **1969**, 42(2), 181-185.
5. R. Atchudan, T. Nesakumar, J. I. Edison, S. Perumal, N. Karthik, D. Karthikeyan, M. Shanmugam, Y. R. Lee, Concurrent synthesis of nitrogen-doped carbon dots for cell imaging and ZnO@ nitrogen-doped carbon sheets for photocatalytic degradation of methylene blue, *J. Photochem. Photobio. A: Chem.*, **2018**, 75-85.
6. Saad S M Hassan, Waleed I M El Azab, Hager R Ali, Mona S M Mansour, Green synthesis and characterization of ZnO nanoparticles for photocatalytic degradation of anthracene, *Adv. Nat. Sci.: Nanosci. Nanotechnol.* **2015**, 6, 3-29.
7. K. L. Bae, J. Kim, C. K. Lim, K. M. Nam, H. Song, Colloidal zinc oxide-copper(I) oxide nanocatalysts for selective aqueous photocatalytic carbon dioxide conversion into methane, *Nature Communications*, **2017**, 8, 1156-1163.
8. S. S. Turkyılmaz, N. Guy, M. Ozacar, Photocatalytic efficiencies of Ni, Mn, Fe and Ag doped ZnO nanostructures synthesized by hydrothermal method: The synergistic/antagonistic effect between ZnO and metals, *J. Photochem. Photobio. A: Chem*, **2017**, 341, 39-50.
9. L. Lu, L. Jing, Z. Yang, G. Yang, C. Wang, J. Wang, H. Wang, and Q. Jiang, One-step in situ growth of ZnS nanoparticles on reduced graphene oxides and their improved lithium storage performance using sodium carboxymethyl cellulose binder, *RSC Advances*, **2018**, 8(17), 9125-9133.
10. H. Razavi-Khosroshahi, K. Edalati, J. Wu, Y. Nakashima, M. Arita, Y. Ikoma, M. Sadakiyo, Y. Inagaki, A. Staykov, M. Yamauchi, and Z. Horita, Z., High-pressure zinc oxide phase as

visible-light-active photocatalyst with narrow band gap. *Journal of Materials Chemistry A*, **2017**, 5(38), 20298-20303.
11. D. Hong, W. Zang, X. Guo, Y. Fu, H. He, J. Sun, L. Xing, B. Liu, X. Xue, High piezo-photocatalytic efficiency of CuS/ZnO nanowires using both solar and mechanical energy for degrading organic dye, *ACS Appl. Mater. Interfaces*, **2016**, 8 (33), 21302-21314.
12. S. Thangavel, K. Krishnamoorthy, V. Krishnaswamy, N. Raju, S.J. Kim, G. Venugopal, Graphdiyne–ZnO nanohybrids as an advanced photocatalytic material, *J. Phys. Chem. C*, **2015**, 119(38), 22057-22065.
13. U. Alam, A. Khan, D. Ali, D. Bahnemann, M. Muneer, Comparative photocatalytic activity of sol–gel derived rare earth metal (La, Nd, Sm and Dy)-doped ZnO photocatalysts for degradation of dyes, *RSC Adv.*, **2018**, 8, 17582-17594.
14. Y. Bao, C. Feng, C. Wang, J. Ma, One-step hydrothermal synthesis of hollow ZnO microspheres with enhanced performance for polyacrylate, *Progress in Organic Coatings*, **2017**, 112, 270-277.
15. J. Zhang, X. Fu, H. Hao, W. Gan, Facile synthesis 3D flower-like Ag@WO_3 nanostructures and applications in solar-light photocatalysis, *J. Alloys Compd*, **2018**, 757, 134-141.
16. C. Wang, M. Wu, M. Yan, H. Shen, F. Cai, B. Hu, W. Shi, Enhanced visible-light photocatalytic activity and the mechanism study of WO_3 nanosheets coupled with Ag_3PO_4 nanocrystals, *Ceram. Inter.*, **2015**, 41, 6784-6792.
17. Q. W. Cao, Y. F. Zheng, X. C. Song, Enhanced visible-light-driven photocatalytic degradation of RhB by $AgIO_3$/WO_3 composites, *J. Taiwan Inst. Chem. Eng.*, **2017**, 70, 359-365.
18. L. Wang, J. Liu, Y. Wang, X. Zhang, D. Duan, C. Fan, Y. Wang, Insight into the enhanced photocatalytic performance of Ag_3PO_4 modified metastable hexagonal WO_3. *Colloids and Surfaces A: Physicochemical and Engineering Aspects*, **2018**, 541, 145-153.
19. T. Wang, W. Quan, D. Jiang, L. Chen, D. Li, S. Meng, M. Chen, Synthesis of redox-mediator-free direct Z-scheme AgI/WO_3 nanocomposite photocatalysts for the degradation of tetracycline with enhanced photocatalytic activity, *Chem. Eng. J.*, **2016,** 300, 280-290.
20. H. Xu, H. Zhao, Y. Xu, Z. Chen, L. Huang, Y. Li, Y. Song, Q. Zhang, H. Li, Three-dimensionally ordered macroporous WO_3 modified Ag_3PO_4 with enhanced visible light photocatalytic performance. *Ceram. Inter*., **2016**, 42, 1392-1398.
21. J. Lu, Y. Wang, F. Liua, L. Zhang, S. Chai, Fabrication of a direct Z-scheme type WO_3/Ag_3PO_4 composite photocatalyst with enhanced visible-light photocatalytic performances, *Appl. Surf. Sci.*, **2017**, 393, 180-190.
22. K. Kaviyarasu, N. Geetha, K. Kanimozhi, C. Maria Magdalane, S. Sivaranjani, A. Ayeshamariam, J. Kennedy, and M. Maaza, In vitro cytotoxicity effect and antibacterial performance of human lung epithelial cells A549 activity of zinc oxide doped TiO_2 nanocrystals: investigation of bio-medical application by chemical method, *Materials Science and Engineering C*, **2017**, 74, 325-333.
23. X. Yuan, L. Jiang, X. Chen, L. Leng, H. Wang, Z. Wu, T. Xiong, J. Liang, G. Zeng, Highly efficient visible-light-induced photoactivity of Z-scheme Ag_2CO_3/Ag/WO_3 photocatalysts for organic pollutant degradation, *Environmental Science: Nano*, **2017**, 4(11), 2175-2185.
24. M. Yan, Y. Wu, F. Zhu, Y. Hu, W. Shi, The fabrication of a novel Ag_3VO_4/WO_3 heterojunction with enhanced visible light efficiency in the photocatalytic degradation of TC, *Phys. Chem. Chem. Phys.*, **2016**, 18, 3308-3315.
25. R. Adhikari, G. Gyawali, T. Sekino, S.W. Lee, Microwave assisted hydrothermal synthesis of Ag/AgCl/WO_3 photocatalyst and its photocatalytic activity under simulated solar light, *J. Solid State Chem.*, **2013**, 197, 560-565.
26. G. Zhu, W. Que and J. Zhang, Synthesis and photocatalytic performance of Ag-loaded β-Bi_2O_3 microspheres under visible light irradiation. *Journal of Alloys and Compounds*, **2011**, 509, 9479-9486.
27. Y. Li, Z. Zhang, Y. Zhang, X. Sun, J. Zhang, C. Wang, Z. Peng and H. Si, Preparation of Ag doped Bi_2O_3 nanosheets with highly enhanced visible light photocatalytic performances, *Ceramics International*, **2014**, 40, 13275-13280.

28. H.-Y. Jiang, K. Cheng, J. Lin, Crystalline metallic Au nanoparticle-loaded α-Bi_2O_3 microrods for improved photocatalysis, *Physical Chemistry Chemical Physics*, **2012**, 14, 12114-12121.
29. J. Zhu, S. Wang, J. Wang, D. Zhang, H. Li, Highly active and durable Bi_2O_3/TiO_2 visible photocatalyst in flower-like spheres with surface-enriched Bi_2O_3 quantum dots. *Applied Catalysis B: Environmental*, **2011**, 102, 120-125.
30. J. Chen, S. Qin, Y. Liu, F. Xin, X. Yin, Preparation of a visible light-driven Bi_2O_3–TiO_2 composite photocatalyst by an ethylene glycol-assisted sol–gel method, and its photocatalytic properties,. *Research on Chemical Intermediates*, **2014**, 40, 637-648.
31. A. Qurashi, Z. Zhong, M. W. Alam, Synthesis and photocatalytic properties of α-Fe_2O_3 nanoellipsoids, *Solid State Sciences*, **2010**, 12(8), 1516-1519.
32. Chunwen Sun, Hong Li, Huairuo Zhang, Zhaoxiang Wang and Liquan Chen, Controlled synthesis of CeO_2 nanorods by a solvothermal method, *Nanotechnology*, **2015**, 16(9), 1454-1465.
33. Ranbo Yu, Lai Yan, Peng Zheng, Jun Chen and Xianran Xing, Controlled synthesis of CeO_2 flower-like and well-aligned nanorod hierarchical architectures by a phosphate-assisted hydrothermal route, *The Journal of Physical Chemistry C*, **2008**, 112(50), 19896-19900.
34. Zhong Lin Wang and Xiangdong Feng, Polyhedral shapes of CeO_2 nanoparticles, *The Journal of Physical Chemistry B*, **2003**, 107(49), 13563-15566.
35. Rui-Juan Qi, Ying-Jie Zhu, Guo-Feng Cheng and Yue-Hong Huang, Sonochemical synthesis of single-crystalline $CeOHOCO_3$ rods and their thermal conversion to CeO_2 rods, *Nanotechnology*, **2005**,16 (11), 2502-2508.
36. S. Kawi, Y. P. Tang, K. Hidajat, L. E. Yu, Synthesis and characterization of nanoscale CeO_2 catalyst for deNO_x, *Journal of Metastable and Nanocrystalline Materials*, **2005**, 23, 95-98.
37. Sumalin Phokha, Supree Pinitsoontorn, Prae Chirawatkul, Yingyot Poo-arporn, Santi Maensiri. "Synthesis, characterization, and magnetic properties of monodisperse CeO_2 nanospheres prepared by PVP-assisted hydrothermal method, *Nanoscale research letters*, **2012**, 7(1), 425-434.
38. Chunwen Sun, Hong Li, ZhaoXiang Wang, Liquan Chen and Xuejie Huang, Synthesis and characterization of polycrystalline CeO_2nanowire, *Chemistry Letters*, **2004**, 33(6), 662-663.
39. Kenji Kaneko, Koji Inoke, Bert Frietag, Ana B Hungria, Paul A Midgley, Thomas W Hansen, Jhing Zhang, Satoshi Ohara and Tadafumi Adschiri, Structural and morphological characterization of cerium oxide nanocrystals prepared by hydrothermal synthesis, *Nano letters*, **2007**, 7(2), 421-425.
40. A.I.Y. Tok, S.W. Du, F.Y.C. Boey and W.K. Chong, Hydrothermal synthesis and characterization of rare earth doped ceria nanoparticles, *Materials Science and Engineering: A*, 2007, 466(1-2), 223-229.
41. Weijun Deng, Donghui Chen and Liang Chen, Synthesis of monodisperse CeO_2 hollow spheres with enhanced photocatalytic activity, *Ceramics International*, **2015**, 41(9), 11570-11575.
42. P. Ji, J. Zhang, F. Chen, and M. Anpo, Ordered mesoporous CeO2 synthesized by nanocasting from cubic Ia3d mesoporous MCM-48 silica: formation, characterization and photocatalytic activity. *The Journal of Physical Chemistry C*, **2008**, 112(46), 17809-17813.
43. Chenguo Hu, Zuwei Zhang, Hong Liu, Puxian Gao and Zhong Lin Wang, Direct synthesis and structure characterization of ultrafine CeO_2 nanoparticles, *Nanotechnology*, **2006**, 17(24), 5983-5993.
44. Shuang Song, Lejin Xu, Zhiqiao He, Jianmeng Chen, XiuzhenXioa and Bing Yan, Mechanism of the photocatalytic degradation of CI Reactive Black 5 at pH 12.0 using $SrTiO_3/CeO_2$ as the catalyst, *Environmental science and technology*, **2007**, 41(16), 5846-5853.
45. Carla A. Orge, Jose JM Orfao, Manuel FR Pereira, Andrea M. Duarte de Farias, Raimundo C. Rabelo Neto and Marco A. Fraga, Ozonation of model organic compounds catalyzed by nanostructured cerium oxides, *Applied catalysis B: Environmental*, **2011**, 103(1-2), 190-199.
46. Jian Tian, Yuanhua Sang, Zhenhuan Zhao, Weijia Zhou, Dongzhou Wang, Xueliang Kang, Hong Liu, Jiyang Wang, Shaowei Chen, Huaqiang Cai and Hi Huang, Enhanced photocatalytic performances of CeO_2/TiO_2 nanobelt heterostructures, *Small*, **2013**, 9(22), 3864-3872.

47. G. Vimal, Kamal P. Mani, Dinu Alexander, P. P. Biju, N. V. Unnikrishnan, M. A. Ittyachen, Cyriac Joseph, Facile synthesis of Sm^{3+}/Eu^{3+} codoped CeO_2 ultrafine nanocrystals and oxygen vacancy site dependent photoluminescence, *Optical material*, **2015**, 50, 220-228.
48. Daotong You, Bao Pan, Fan Jiang, Yangen Zhou and Wenyue Su, Cds nanoparticles/CeO_2 nanorods composite with high-efficiency visible-light-driven photocatalytic activity, *Applied Surface Science*, **2016**, 363, 154-160.
49. Yongbao Liu, Gangqiang Zhu, JianZhi Gao, Mirabbos Hojamberdiev, Hongbin Lu, Runliang Zhu, Xiumei Wei and Peng Liu, A novel $CeO_2/Bi_4Ti_3o_{12}$ composite heterojunction structure with an enhanced photocatalytic activity for bisphenol A, *Journal of Alloys and Compounds*, **2016**, 688, 487-496.
50. Chanmine Lee, Yukwon Jeon, Taehyen Kim, Akihiro Tou, Joo-II Park, Hisahiro Einaga and Yong-Gun Shul, Ag-loaded cerium-zirconium solid solution oxide nano-fibrous webs and their catalytic activity for soot and CO oxidation, *Fuel*, **2008**, 212, 395-404.
51. Xiaowang Lu, Xiazhang Li, Junchao Qian and Zhingang Chen, The surfactant-assisted synthesis of CeO_2 nanowires and their catalytic performance for CO oxidation, *Powder Technology*, **2013**, 239, 415-421.
52. Ting Chen, Zhixiang Xie, Weihui Jiang, Wan Jiang, Xiaojun Zhang and Jianmin Liu, Synthesis of CeO_2 nanosheets with a room temperature ionic liquid assisted method, *Journal of advanced ceramics*, **2016**, 5(2), 111-116.
53. Tarek Alammar, Heshmat Noei, Yuemin Wang, Wolfgang Grunert and Anja-Verena Mudring, Ionic liquid-assisted sonochemical preparation of CeO_2 nanoparticles for CO oxidation, *ACS Sustainable Chemistry and Engineering*, **2014**, 3(1), 42-54.
54. Natda Wetchakun, Saranyoo Chaiwichain, Burapat Inceesungvorn, Kanlaya Pingmuang, Sukon Phanichphant, Andrew I Minett and Jun Chen, $BiVO_4/CeO_2$ nanocomposites with high visible-light-induced photocatalytic activity, *ACS applied materials and interphases*, **2012**, 4(7), 3718-1723.
55. Yangang Wang, Fei Wang, Yuting Chen, Daofang Zhang, Bo Li, Shifei Kang, Xi Li and Lifeng Cui, Enhanced photocatalytic performance of ordered mesoporous Fe-doped CeO_2 catalyst for the reduction of CO_2 with H_2O under simulated solar irradiation, *Applied Catalysis B: Environmental*, **2014**, 147, 602-609.